IOP Conf. Series: Materials Science and Engineering **117** (2016) 012029 doi:10.1088/1757-899X/117/1/012029

Applications of the directional solidification in magnetic shape memory alloys

Y J Huang[1], J Liu[2], Q D Hu[1], Q H Liu[1], I Karaman[3,4] and J G Li[1,a]
[1] School of Materials Science and Engineering, Shanghai Jiao Tong University, Shanghai 200240, China
[2] Key laboratory of Magnetic Materials and Devices, Ningbo Institute of Material Technology and Engineering, CAS, Ningbo 315201, China
[3] Department of Mechanical Engineering, Texas A&M University, College Station, TX 77843, USA
[4] Department of Material Science and Engineering, Texas A&M University, College Station, TX 77843, USA

E-mail: [a]lijg@sjtu.edu.cn

Abstract. A zone melting liquid metal cooling (ZMLMC) method of directional solidification was applied to prepare highly-oriented $Ni_{52}Fe_{17}Ga_{27}Co_4$ magnetic shape memory alloys. At high temperature gradient and low growth velocity, the well-developed preferred orientation for coarse columnar crystals was obtained. Such a structure leads to a large complete pseudoelastic recovery of 5% at 348 K. Moreover, the pseudoelastic behaviours and the kinetics of the martensitic transformation (MT) are significantly affected by the intersection angle between the loading direction and the grain boundaries.

1. Introduction

Magnetic shape memory alloys (MSMAs) have been considered as potential substitutes for giant magnetostrictive and piezoelectric materials in actuator application because they exhibit a large magnetic field induced strain (MFIS) of up to 10% [1]. Moreover, in comparison with other conventional shape memory alloys (SMAs), MSMAs show a better combination of high strain and high actuation frequencies, which has led to the search for new MSMAs including Ni-Mn-X (X=Ga, In, Sn, Sb) [2, 3], Ni-Fe-Ga-(Co) [4] and Co-Ni-Al [5] alloys. Among them, Ni-Fe-Ga-(Co) MSMAs with an significantly improved ductility [4, 6] are regarded as a promising candidate owing to low field requirement for triggering MFIS [7], and high magneto-crystalline anisotropy energy [8]. Interestingly, the MT temperatures and Curie temperature of Ni-Fe-Ga-(Co) FSMAs can be tailored over a wide range via compositional modifications and heat treatments [9, 10]. More importantly, a relatively large MFIS was obtained in Ni-Fe-Ga-(Co) alloys at room temperature [7]. Experimental and theoretical transformation strains for Ni-Fe-Ga-(Co) alloys exceed that in most other commercial SMAs [11]. Additionally, Ni-Fe-Ga single crystals can exhibit complete pseudoelastic recovery over a wide temperature range (>300 K) as compared to other SMAs [12]. Large, fully recoverable tensile strains greater than 10% have been measured in selected single crystal orientations [13].

However, their excellent functional properties are usually achieved in the single crystals [1, 14], which is difficult and time consuming. Fortunately, recent documents show that a large reversible magnetic field-induced strain could be achieved in highly textured polycrystals [15, 16], as the

anisotropy of such a structure is analogous to that of single crystals, which can be prepared by the directional solidification [17]. Therefore, one aim of this work is to obtain such highly textured polycrystals of $Ni_{52}Fe_{17}Ga_{27}Co_4$ MSMA by using directional solidification. Meanwhile, the role of grain boundary on the MT in this kind of MSMAs is still unclear because previous investigations mainly focus on single crystals. Therefore, another purpose of this work is to study the role of grain boundary on pseudoelastic behaviours in highly-oriented polycrystals.

2. Experimental

Homogeneous ingots with nominal composition of $Ni_{52}Fe_{17}Ga_{27}Co_4$ (in at. %) were firstly prepared from Ni, Fe, Ga, Co (all 99.99% purity) by arc melting four times and then cast into a graphite cylinder mold. Subsequently, directional solidification was carried out in the self-made ZMLMC furnace. The process of the directional solidification has been described in details elsewhere [17]. In this work, the directionally solidified $Ni_{52}Fe_{17}Ga_{27}Co_4$ samples were conducted at three different parameters: (i) G_L=250 K/cm, V=100 μm/s; (ii) G_L=1200 K/cm, V=15 μm/s; (iii) G_L=1200 K/cm, V=5 μm/s.

The crystal structure and preferred orientation was identified by X-ray diffraction analysis (XRD; Rigaku, Ultima IV) using Cu K_α radiation. Microstructure was investigated by optical microscopy (OM; Axio Imager A1m).

To test the role of grain boundary on the MT, compression samples were cut from the directionally solidified rods into rectangular prisms with nominal dimensions of 3mm×3mm×6mm, and with one of the three different intersection angles between the compression axis and the crystal growth direction (CGD). It should be noted that, for better understanding the role of grain boundaries, all specimens were used in as-cast form without any heat treatments to avoid precipitation of γ phase [9] and cut from the same rod that was directionally solidified at the condition (iii). Figure 1 shows the loading and crystal growth directions for samples cut at 0°, 45° and 90°. The compression experiments were conducted using an MTS screw driven test frame with a heating/cooling rate of 10 K/min. A high temperature extensometer was used to measure the strain from the tips of the compression platens. After compression, the surface topography was observed by OM.

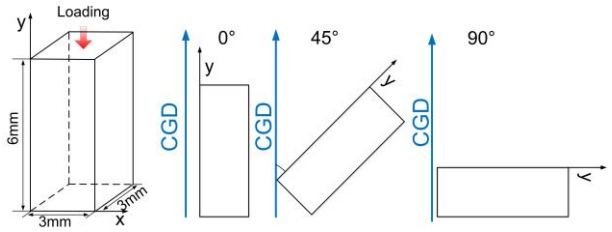

Figure 1. Schematics of the compressive samples and their crystal growth direction (CGD).

3. Results and discussions

3.1 Microstructure of the directionally solidified samples

Figure 2a shows the XRD patterns a transverse section of the arc-melting master alloys and the directionally solidified samples. The master alloys show the random orientations of $L1_0$ martensite [9], which is in accordance with the microstructural observation indicating the typical equiaxial grains (figure 2b). As for the directionally solidified samples, at condition (i), two peaks of (004) and (440) $L1_0$ are detected at 56.6° and 69.5°, respectively. Additionally, there are small signals of (220) and (222) $L1_0$. However, at condition (ii) and (iii), only one sharp peak of (222) $L1_0$ at 43.5° is observed. It is suggested that the preferred orientation of the (222) $L1_0$ is well developed at high G_L and low V. On the other hand, the microstructure of steady growth zones in the longitudinal section shows that six columnar grains grow along the rod axis at condition (i) (figure 2c). In contrast, at condition (ii), only three columnar grains containing some large martensitic blocks can be observed (figure 2d); at condition (iii), only two columnar grains can be observed in the longitudinal section (figure 2e).

Moreover, some differently shaped martensitic lamellae are exhibited in different blocks (figure 2d). Micro-twinning substructures are found between the parallel martensitic lamellae, which have been studied by the electron backscatter diffraction (EBSD) [18].

Generally, highly crystal anisotropy leads to the high energy of magnetocrystalline anisotropy [19], which is a key to obtain large MFIS [1, 8]. However, magnetic anisotropy is usually dissipated in multi-variant state, which is induced by the self-accommodating manner when the MT occurs. Therefore, it is very meaningful that the whole columnar grain (figure 2e) is occupied by one large martensitic block, so called the giant single-variant set, in this case where uniformly oriented martensitic lamellae are well aligned. Subsequently, we will present the superelasticity behaviours in such a highly-oriented structure.

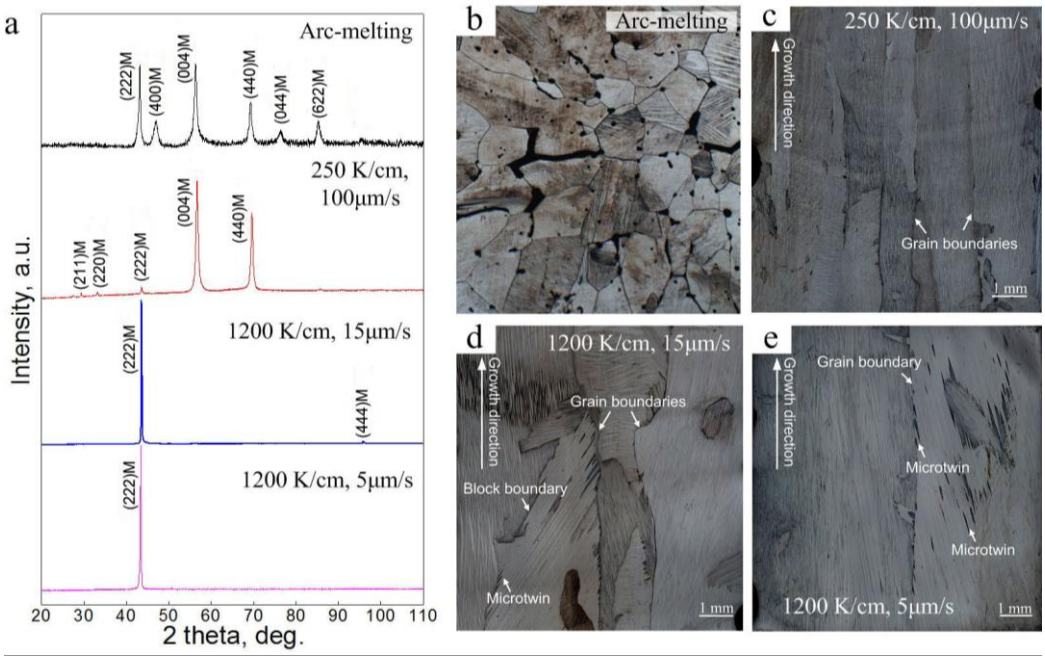

Figure 2. (a) XRD patterns of the transverse section of the master alloy and the directionally solidified samples, (b-e) the corresponding microstructure for the arc-melting (b) and longitudinal section morphology of the steady growth zone in directionally solidified samples under various conditions: (c) G_L=250 K/cm, V=100 μm/s, (d) G_L=1200 K/cm, V=15 μm/s, (e) G_L=1200 K/cm, V=5 μm/s.

3.2 Pseudoelastic behaviours

Before the compression tests, the martensitic start (M_s = 336 K) and finish (M_f = 326 K) temperatures and the austenite start (A_s = 337 K) and finish (A_f = 348 K) temperatures were determined using differential scanning calorimetry (DSC, NETZSCH) with a heating/cooling rate of 10 K/min.

The compressive stress-strain responses for three orientations at 348K (A_f) are shown in figure 3. A complete pseudoelastic recovery is found for the 0° samples when loaded to 5% strain (figure 3a). This strain magnitude is comparable to that of other single crystalline MSMAs (6.5% for $Ni_{49}Fe_{18}Ga_{27}Co_6$ [20], 4.2% for $Ni_{54}Fe_{19}Ga_{27}$ [21], 5% for $Ni_{53.1}Mn_{26.6}Ga_{20.3}$ [22], etc.). The onset stress (σ_s) for the inelastic deformation stage is steady at 56 MPa until the fifth cycle. On the fifth cycle, σ_s drops to 40 MPa, and the stress hysteresis ($\Delta\sigma$) increases by 32 MPa. This implies that no cyclic hardening is produced as observed in NiFeGa [12], and a good compatibility of strain at the grain boundaries is satisfied at the angle of 0°.

For the other two samples (45° and 90°), partial pseudoelastic recovery is observed (figure 3b and c). On the first loading cycle for the 45° sample, a residual strain of 0.61% is recorded after a recovery of 0.39% upon unloading. Of the recovered strain, 0.12% is ascribed to the elastic recovery (ε_{el}) using

an apparent elastic modulus of 29 GPa for the martensite, and the remaining 0.27% (ε_M) is apparently associated with the reverse transformation to austenite. On subsequent cycles, the ε_M decreases, which is attributed to the microstrain accumulated in the vicinity of grain boundaries during the cyclic loading. This suggests that the strain compatibility at the grain boundaries is reduced. A similar phenomenon is also evident in the 90° samples (figure 3c). It is noted that the compressive stress level of the 45° sample is close to half that in the 0° and 90° samples, which may be attributed to the greater Schmid factor and more active correspondent variant pairs (CVPs) [12].

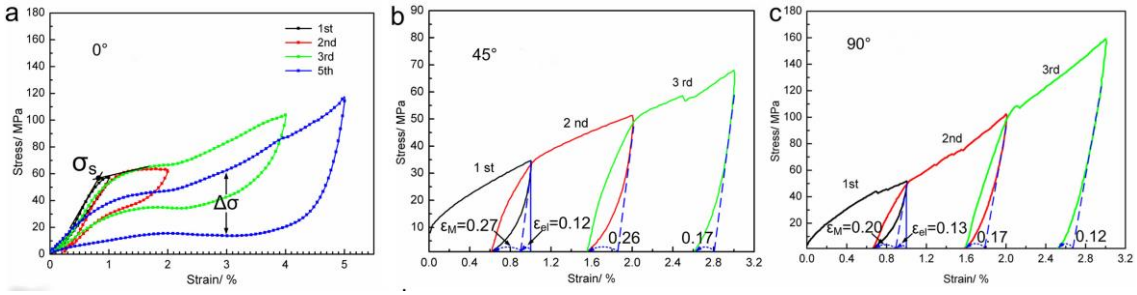

Figure 3. The compressive stress-strain responses at A_f = 348 K: (a) 0°, (b) 45°, (c) 90° samples.

To further investigate the effects of grain boundaries and angles with loading direction, the surface topography for the compressed samples after testing are presented in figure 4. From the enlarged images around the grain boundaries (figure 4d, e and f), for the 0° samples, needle- or plate-like martensite variants are symmetrically formed and then grow into the parent phase (the white arrows in figure 4d). Such morphology minimizes the elastic strain energy generated during the MT and provides a good strain compatibility of the grain boundaries. In addition, for the 45° samples, more fine multi-variant lamellae are resulted from the self-accommodation mechanism [23] (figure 4e). As the intersection angle increases to 90°, some cracks are produced at triple junctions (figure 4c and f). Also, coarse martensite lamellae are formed in the grains at two ends of the samples (A in figure 4f), while the austenite phase is retained in the central grains (B and C in figure 4f).

It is clear that from the aforementioned results, the angle between grain boundaries and the loading direction has a critical role on the MT. Meanwhile, those phenomena suggest that there is a stress field surrounding the grain boundaries, which leads to a certain incompatibility across grain boundaries. Based on the geometric mechanics, the applied stress on grain boundary plane can be divided into two parts of the shear stress and the compressive stress (figure 5a). Moreover, the resolved compressive stress increases as the intersection angle (ɵ) increases. The resolved shear stress promoting the growth of the martensite is hardly constrained by the grain boundaries [24]. In contrast, the transport of the resolved compressive stress across the grain boundaries is easier to be hindered.

For the intersection angle of 0°, it is reasonable to deduce that the compressive stress at grain boundaries is lower and the strain compatibility in neighbouring grains is better. In other words, when each single grain is transformed to various variants, the same displacement in each grain is generated on the grain boundary plane (figure 5b). Thus, the symmetrical morphology of martensite is formed in the neighbouring grains near the grain boundaries (figure 4d), and the complete pseudoelastic recovery of 5% is obtained at the angle of 0° (figure 3a).

The resolved compressive stress on the grain boundary plane for the angle of 90° is the larger. Furthermore, the buffering effect of the grain boundaries for transporting the applied stress leads to stress concentrations at grain boundaries. Thus, during the cyclic loading, the applied stress in the grains at two ends of the 90° samples increases more quickly than that of the central grains. This suggests that the martensitic phase firstly nucleates at grain boundaries and preferably grows into the grains at two ends (figure 4f). At the beginning of the MT, in order to maintain the strain continuity at the boundary plane, the central grains are required to accommodate plastically because their free energy for the MT is not satisfied, as schematized by figure 5c showing the strain incompatibility on the grain boundary plane. On subsequent loading, the plastic deformation may be produced in the

vicinity of grain boundaries, because the potency of the boundaries as nucleation sites for the martensite is always reduced by the prior deformation, even if it has been small. It should be noted that a large stress concentration (indicated by the white dot circles in figure 4c) would be formed by the plastic deformation at the crystal defects, especially at the triple junctions, and then lead to the cracks (figure 4f). As a result, a high fraction of retained austenite phase is observed in the central grains (figure 4c and f) while the coarse martensite lamellae in the grains at two ends, and only partial pseudoelastic recovery is presented (figure 3c). It is reasonable to infer that a similar effect is also presented in the 45° samples, reducing the strain compatibility across grain boundaries because the resolved compressive stress is between that of the 90° and 0° samples (figure 5a).

On the other hand, two kinetic roles of the stress concentrations on the MT should be considered. One is to activate additional slip, leading to different displacement in neighbouring grains (figure 5c) and asymmetric morphology (figure 4f). Another is to decrease the non-chemical free energy required for the MT, promoting the nucleation of the martensite and resulting in an apparent increase of the MT temperatures [24]. Thus, it is reasonable to conclude that the M_s of the 90° samples is shifted to a higher temperature. In other words, the compression temperature (348 K) for the 90° samples may be below its M_s, resulting in the partial pseudoelastic recovery. The compressive strain – temperature curves at a constant stress of 50 MPa (figure 6) show that the MT temperatures for the 90° samples are higher by 17 K than that for the 0° samples. Note that their MT temperatures without external stress field are very close to each other (Inset in figure 6). A lower transformation strain for the 90° samples is also presented due to the strain incompatibility at the grain boundaries.

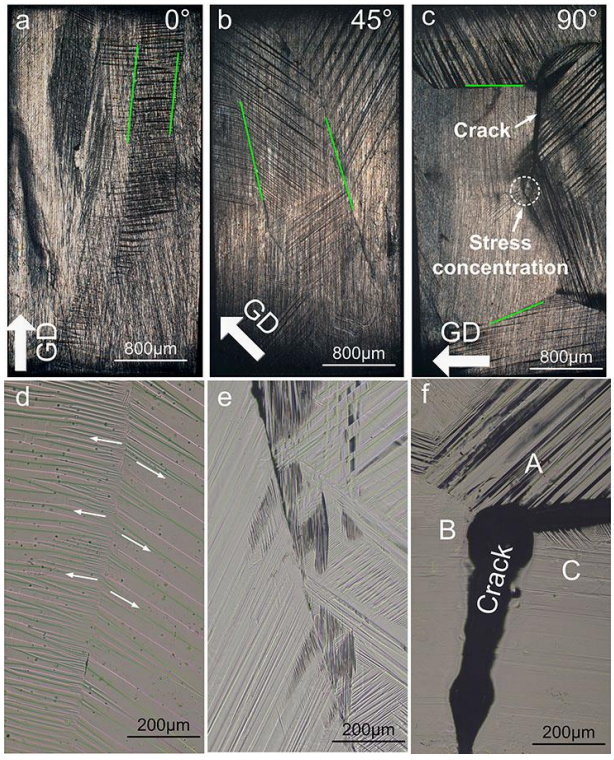

Figure 4. Optical images of surface topography for the compressed samples: (a, d) 0°, (b, e) 45°, (c, f) 90°. The enlarged images around grain boundaries (d, e and f) correspond to (a, b and c), respectively. The green lines indicate the grain boundaries.

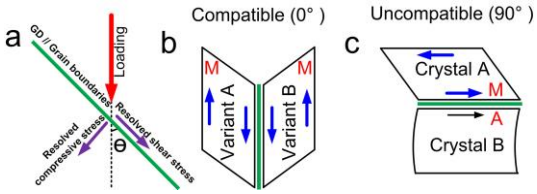

Figure 5. (a) A schematic of the stress distributions in the stress field surrounding the grain boundaries (green lines); (b) and (c) schematics of the relationship between the strain compatibility at grain boundaries, corresponding to 0° and 90°, respectively. The red letters of "M" stand for the martensitic phase.

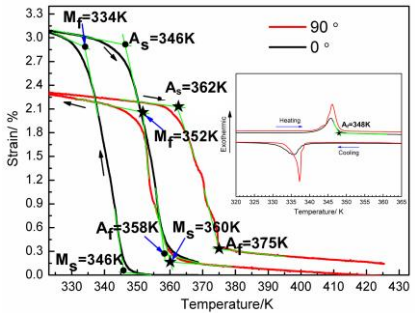

Figure 6. The compressive strain–temperature curves at a constant stress of 50 MPa. Inset shows that their MT temperatures determined by DSC, which are very close to each other

4. Conclusion

The ZMLMC directional solidification was successfully applied to obtain highly oriented polycrystals of $Ni_{52}Fe_{17}Ga_{27}Co_4$ MSMAs. The solidification conditions have a great influence on the microstructure and crystal orientation of alloys. At G_L=1200 K/cm and V=5 μm/s, columnar tricrystal with giant martensitic single-variant sets is obtained. Such a highly-oriented structure results in a complete pseudoelastic recovery of 5% at 348 K when loaded to the crystal growth direction (0°). At higher intersection angles (45° and 90°) between the loading direction and the grain boundaries (the crystal growth direction), only partial pseudoelastic recovery is observed. In comparison with the 0° samples, the MT temperatures under stress for the cases with the intersection angle of 90° are higher. The microstructural observation shows that different martensite morphologies are formed for different intersection angles.

Acknowledgements

This work was financially supported by the National Natural Science Foundation of China (Grant nos. 51010425 and 51027005). The authors are grateful to Instrumental Analysis Center of Shanghai Jiao Tong University for technical support. I.K. acknowledges the financial support from U.S. National Science Foundation, Division of Materials Research, Metals and Metallic Nanostructures Program, Grant No. 1108396, under the umbrella of Materials World Network Initiative.

References

[1] Sozinov A, Likhachev A A, Lanska N and Ullakko K, 2002 *Appl. Phys. Lett.* **80** 1746
[2] Sutou Y, Imano Y, Koeda N, Omori T and Kainuma R, et al, 2004, *Appl. Phys. Lett.* 85 4358
[3] Huang Y J, Hu Q D and Li J G, 2012 *Appl. Phys. Lett.* **101** 222403
[4] Font J, Muntasell J, Santamarta R and Masdeu F, et al, 2006 *Mater. Sci. Eng. A* **438-440** 919.
[5] Liu J and Li J G, 2006 *Scr. Mater.* **55** 755
[6] Sui J, Gao Z, Yu H, Zhang Z and Cai W, 2008 *Scr. Mater.* **59** 874
[7] Morito H, Oikawa K, Fujita A, Fukamichi K and Kainuma R, et al, 2005 *Scr. Mater.* **53** 1237
[8] Morito H, Fujita A, Oikawa K, Fukamichi K, Kainuma R, Kanomata T and Ishida K, 2009 *J. Phys.: Condens. Matter.* **21** 076001
[9] Liu J, Scheerbaum N, Hinz D, Gutfleisch O, 2008 *Acta Mater.* **56** 3177
[10] Liu J, Scheerbaum N, Gutfleisch O, 2008 *IEEE Trans. Magn.* **44** 3025
[11] Hamilton R F, Sehitoglu H, Chumlyakov Y and Maier H J, 2004 *Acta Mater.* **52** 3383
[12] Efstathiou C, Sehitoglu H, Kurath P, Foletti S and Davoli P, 2007 *Scr. Mater.* **57** 409
[13] Hamilton R F, Sehitoglu H, Efstathiou C and Maier H J, 2007 *Acta Mater.* 55 4867
[14] Pötschke M, Weiss S, Gaitzsch U, Cong D, Hürrich C and Roth S, et al 2010 *Scr. Mater.* **63** 383
[15] Liu J, Aksoy S, Scheerbaum N, Acet M and Gutfleisch O, 2009 *Appl Phys Lett* **95** 232515
[16] Gaitzsch U, Potschke M, Roth S, Rellinghaus B and Schultz L, 2009 *Acta Mater.* **57** 365
[17] Huang Y J, Hu Q D, Liu J, Zeng L, Zhang D F, Li J G, 2013 *Acta Mater.* **61** 5702
[18] Liu Q H, Liu J, Huang Y J, Hu Q D and Li J G, 2013 *J. Alloys Compd.* **572** 186
[19] Morito H, Fujita A, Fukamichi K and Kainuma R, et al, 2002 *Appl. Phys. Lett.* **81** 1657
[20] Panchenko E, Chumlyakov Y, Maier H J and Timofeeva E, et al, 2010 *Intermetallics* **18** 2458
[21] Chumlyakov Y, Panchenko E, Kireeva I, Karaman I, Sehitoglu H, Maier H J, Tverdokhlebova A and Ovsyannikov A, 2008 *Mater. Sci. Eng., A* **481–482** 95
[22] Chernenko V A, L'vov V, Pons J and Cesari E, 2003 *J. Appl. Phys.* **93** 2394
[23] Yamanaka A, Takaki T and Tomita Y, 2010 *Int. J. Mech. Sci.*, **52** 245
[24] Ueda M, Yasuda H Y and Umakoshi Y, 2001 *Acta Mater.* **49** 3421